REVISTA CUBANA DE CIENCIAS BIOLÓGICAS
http://www.rccb.uh.cu

ARTÍCULO ORIGINAL

Rational approach of the structure-function relationship using chimeric isoforms provides new insights into the functional differences of sticholysins

Un enfoque racional de la relación estructura-función con el uso de isoformas quiméricas de sticholysinas proporciona nuevas consideraciones sobre sus diferencias funcionales

Aisel Valle Garay [1,2], Jose Antonio Pereiro-Morejón[1], Luis Benito Pérez-Socas[1], Yadira de la Patría Hervis Valdés[1], Liem Canet Santos[1], Heidy González-Alvarez[1], Camilo Ayra-Pardo[3,4], Isabel Fabiola Pazos Santos[1]

[1] Centro de Estudio de Proteínas, Facultad de Biología, Universidad de La Habana, Cuba
[2] Laboratoriode Biofísica Molecular, Instituto de Ciencias Biológicas, Universidad de Brasília, DF-Brasília, Brasil.
[3] Centro de Ingeniería Genética y Biotecnología, La Habana, Cuba China-UK-NYNU-RRES Joint
[4] Laboratory of Insect Biology, Nanyang Normal University (NYNU), Henan 473061, P.R. China

*Autor para correspondencia:
aiselvalle@unb.br
aiselvalle@gmail.com

Recibido: 2020-08-10

Aceptado: 2020-10-10

ABSTRACT

Sticholysin I and II are two isoforms of pore-forming proteins from *Stichodactyla helianthus* sea anemone, exhaustively characterized. Sticholysin I and II have 176 and 175 amino acid residues respectively, and only 12 amino acid substitutions. Consequently, these isoforms have 99% of similarity and 93% of identity of sequences with very similar three-dimensional structures. However, sticholysin II is hemolytically more active than sticholysin I on human red blood cells and guinea pig blood cells. The reasons for theses functional differences are not known but interestingly most of the amino acid changes are located in functional regions such as: N-terminal segment, loops associated with membrane binding site, and protein-protein interaction sites. To deepen into the hemolytic activity differences between sticholysin I and II we designed and obtained three chimeric sticholysins in *Escherichia coli* that exchange different segments of both isoforms. The analysis of the hemolytic activity of these chimeras and their homology modeling provided new evidences on the pore-forming activity of actinoporins, as well as on the amino acid residues that could be involved in the functional difference between sticholysins I and II, in the interaction of these proteins with membranes or in the oligomerization process.

Keywords: actinoporin, sticholysin, pore-forming protein, pore-forming mechanism, chimeric protein

RESUMEN

Sticholysinas I y II son dos isoformas de proteínas formadoras de poros de la anémona de mar Stichodactyla helianthus *caracterizadas exhaustivamente. Sticholysinasl y II tienen 176 y 175 residuos de aminoácidos respec-*

tivamente y solo 12 diferencias aminoacídicas. En consecuencia, tienen un 99% de similitud, un 93% de identidad secuencial, y estructuras tridimensionales muy similares. Sin embargo, la sticholysina II es hemolíticamente más activa que la sticholysina I en eritrocitos humanos y de cobayos. No se conocen las razones de estas diferencias funcionales, pero es interesante que la mayoría de los cambios aminoacídicos se encuentran en regiones funcionales como: el segmento N-terminal, los lazos asociados con el sitio de unión a la membrana y los sitios de interacción proteína-proteína. Para profundizar en las diferencias de actividad hemolítica entre las sticholysinas I y II, diseñamos y obtuvimos por vía recombinante en Escherichia coli *tres proteínas quiméricas que intercambian diferentes segmentos de ambas isoformas. El análisis de la actividad hemolítica de estas proteínas quiméricas y su modelación por homología proporcionó nuevas evidencias sobre la actividad formadora de poros de las actinoporinas, así como sobre los residuos aminoacídicos que pudieran estar implicados en la diferencia funcional entre las sticholysinas I y II, en la interacción de estas proteínas con las membranas o en el proceso de oligomerización.*

Palabras claves: *actinoporina, sticholysina, proteína formadora de poros, mecanismo de formación de poros, proteína quimérica.*

INTRODUCTION

Actinoporins are a pore-forming protein (PFP) family produced by sea anemones. The name is due to their purification from the order *Actiniaria* and its ability to form pores in membranes (Kem 1988). Actinoporins are small proteins (~20 kDa) classified as α-type PFP that interact with membrane through α-helical elements (Anderluh and Maček 2002; Alegre-Cebollada *et al.* 2007a).

These proteins have high affinity for sphingomyelin (SM)-containing membranes (Belmonte *et al.* 1994; Tejuca *et al.* 1996; Válcarcel *et al.* 2001; Bakrač *et al.* 2008; Kohno *et al.* 2009) where they form oligomeric pores at nanomolar concentration, leading to target cells lysis. *Stichodactyla helianthus* is a sea anemone abundant in the Caribbean Sea that produces two actinoporin isoforms designated sticholysin I (StI) and II (StII), thoroughly characterized (Lanio *et al.* 2001; Martínez *et al.* 2001; Válcarcel *et al.* 2001; Martinez *et al.* 2007). Besides StI and StII, Equinatoxin II (EqtII) from *Actinia equina* and fragaceatoxin C (FraC) from *Actinia fragacea* are prominent examples of actinoporins family (Tanaka *et al.* 2015; Valle *et al.* 2015; García-Linares *et al.* 2017).

The high cytolytic activity of actinoporin have caught the attention of many researchers for their potential use in the development of molecular tools, with possible medical and biotechnological applications, such as (Ramírez-Carreto *et al.* 2020): immunotoxins construction against tumor cells (Ávila *et al.* 2007; Álvarez *et al.* 2009; Tejuca *et al.* 2009), cytosolic delivery systems for biomolecules like drugs and antigens (Lanio *et al.* 2014), adjuvants (Laborde *et al.* 2017) and for protein-membrane interaction studies (Alegre-Cebollada *et al.* 2007a; Álvarez *et al.* 2009; Valle *et al.* 2011).

The water-soluble and lipid bound complex structures of these actinoporins and several mutants has been solved by NMR and X-ray diffraction (Athanasiadis *et al.* 2001; Hinds *et al.* 2002; Mancheño *et al.* 2003; Kristan *et al.* 2004; Castrillo *et al.* 2009; Mechaly *et al.* 2011; Pardo-Cea *et al.* 2011; Morante *et al.* 2015; Tanaka *et al.* 2015).

Structural superposition of the different actinoporins structures has demonstrated a similar global folding (Mancheño *et al.* 2003; Mechaly *et al.* 2011) showing common structural features with: a β-sandwich fold composed of 10–12 β-strands and flanked by two α-helices. The amphipathic α1-helix is locate in the N-terminal segment and the second short α2-helix in the conserved phosphorylcholine (POC)-binding site (Mancheño *et al.* 2003; Alegre-Cebollada *et al.* 2007a) associated with the membrane interfacial binding site (IBS) (Bakrač *et al.* 2008; Mechaly *et al.* 2011). In addition, crystal structures of the FraC transmembrane pore suggested lipidic multivalence during the actinoporin interaction with membranes by four POC-binding sites (Tanaka *et al.* 2015).

The actinoporin pore-formation mechanism is not completely understood at the molecular level, but a multistep process has been proposed (Hong *et al.* 2002; Malovrh *et al.* 2003; Wacklin *et al.* 2016): i) soluble monomers bind to membrane via a cluster of aromatic amino acids, interfacial binding site (IBS), phosphorylcholine (POC) binding

sites, and basic regions; ii) monomers oligomerize and the N-terminal segment, including amphipathic α1-helix, is separated from the β-sandwich by a pseudo-rigid movement to iii) form the transmembrane pore (Hong *et al.* 2002; Malovrh *et al.* 2003; Mancheño *et al.* 2003; Kristan *et al.* 2004; Alegre-Cebollada *et al.* 2007a; Mechaly *et al.* 2011; García-Linares *et al.* 2013; Rojko *et al.* 2013; Tanaka *et al.* 2015). Despite the determination of the putative transmembrane-pore structure of FraC (Tanaka *et al.* 2015), the oligomerization step is probably the most controversial.

StI and StII have 176 and 175 amino acid residues respectively, and only 12 amino acid substitutions. These isoforms have 99% of similarity and 93% of identity of sequences (Huerta *et al.* 2001; Lanio *et al.* 2001) with very similar threedimensional (3D) structures (Castrillo *et al.* 2009). However, StII is hemolytically more active than StI on human red blood cells (HRBC) (Lanio *et al.* 2001; Álvarez *et al.* 2009; García *et al.* 2009) and guinea pig blood cells (García *et al.* 2009). The reasons for theses functional differences are not known but interestingly most of the amino acid changes (D9/A8, E16/Q15, V63/F62, S77/D76, S78/T77, N95/S94, P122/S121, M135/L134, Y148/H147 and Q149/E148) are located in functional regions such as: N-terminal segment (include α-1 helix), loops associated with membrane binding site, and protein-protein interaction sites (Mancheño *et al.* 2003; Bakrač *et al.* 2008; Mechaly *et al.* 2011; Tanaka *et al.* 2015).

To investigate the different hemolytic activity of StI and StII, we designed and obtained three chimeric sticholysins that exchange different segments of its amino acid sequence.

The analysis of the hemolytic activity of these chimeras was conducted to show that they conserved hemolytic activities with intermediate values between StI and StII. The homology modeling provided new evidences to hypothesize that several semi-conservative and non-conservative amino acid changes between the sticholysin isoforms are important for explaining their functional differences. Specifically, the salt bridge D9-K68 in StI is not sufficient to explain the functional differences between StI and StII isoforms. We indicated that residues H147/E148 of StII are nearby to the protein-protein interface and could also explain the increased hemolytic activity of StII with respect to StI.

MATERIALS AND METHODS

Design of chimeric sticholysins

To rationally design the chimeric forms, StI and StII sequences were divided into three segments, each containing four of 12 amino acid substitutions: (i) the N-terminal, (ii) the middle, and (iii) the C-terminal (Fig.1A and 1B). Three chimeric variants were formed by exchanging these three segments as represented in Fig.1C.

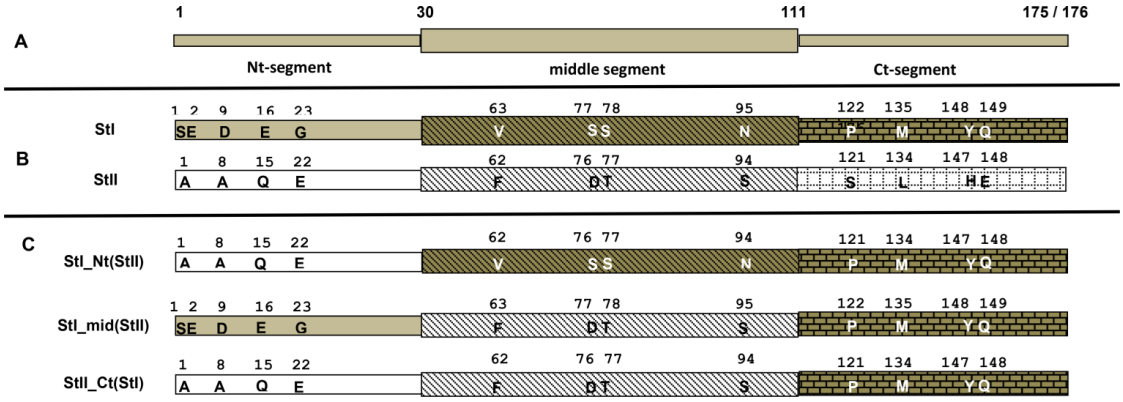

Figure 1. Design of chimeric sticholysins**.** The sequence of StI and StII (176 and 175 residues, respectively) were divided in three segments: the N-terminal (residues 1-30), the middle (residues 31-111), and the C-terminal (residues 112-176/175) (A). The 12 amino acid differences between StI and StII were distributed in order that each segment contains four amino acid substitutions, numbered and identified in StI and StII sequences (B). Three chimeric sticholysin variants exchanging the N-terminal (StI_Nt(StII)), the middle (StI_mid(StII)), and the C-terminal segment (StII_Ct(StI)) were designed (C).

Figura 1*. Diseño de las sticholysinas quiméricas. La secuencia de StI y StII (176 y 175 residuos, respectivamente) se dividió en tres segmentos: el N-terminal (residuos 1-30), el intermedio (residuos 31-111) y el C-terminal (residuos 112-176/175) (A). Las 12 diferencias de aminoácidos entre StI y StII se distribuyeron de forma tal que cada segmento contiene cuatro sustituciones de aminoácidos, numeradas e identificadas en las secuencias de StI y StII (B). Se diseñaron tres variantes quiméricas de sticholysinas que intercambian los segmentos N-terminal (StI_Nt(StII)), el intermedio (StI_mid(StII)) y el C-terminal (StII_Ct(StI)) (C).*

The genes (≈ 500pb) were designed from sequences of sticholysins and the codon usage optimized for *E. coli* expression according to *GenScript* website (*http://www.genscript.com*). Different restriction sites were included for the specific identification of genes. The chimeric genes were synthesized and cloned into *pET3a* expression plasmid by *Genone* company (*http://www.genone.com.br*). Finally, according to the exchanged segments, the three plasmids were named *pET3a-stI_Nt(stII)*, *pET3a-stI_mid(stII)* and *pET3a-stII_Ct(stI)*.

Protein expression and purification

The wild-type sticholysins were purified from the anemone as previously described (Lanio *et al.* 2001). The chimeric sticholysins were expressed by auto induction method (Studier 2005) using *BL21(DE3)*, *BL21 (DE3)pLysS* and *BL21(DE3)pLysE E. coli* strains transformed by heat shock method (Froger and Hall 2007) with the corresponding plasmids. For the study of expression and solubility levels, flasks with 50 mL of autoinduction media (ZYB-5052) were inoculated with non-inducing (MDG) culture from isolated colonies (Studier 2005), and grown overnight at 37 °C and 250 rpm. Colonies with the highest level of soluble protein of interest expression were used for expression in flasks 600 mL autoinduction ZYB-5052 media in the same conditions. Appropriate antibiotic selection was performed for each media. The chimeric proteins were purified from supernatants of lysed bacteria by one-step cation-exchange chromatography using a carboxymethyl cellulose (CM-52 Whatman, USA) column (Pazos *et al.* 2006) in an *ÄKTAprime* system (GE Healthcare Bio-Sciences AB, Sweden) with a linear gradient of 0-100% of 0.5 M NaCl in 0.02 M Na-phosphate, pH 7.4 (PBS buffer). Protein expression and purified proteins were analyzed by sodium dodecyl sulfate polyacrylamide gel electrophoresis (SDS-PAGE) using molecular weigth marker (Laemmli 1970) and purity analyzed by high performance liquid chromatography on a reverse phase (RP-HPLC). Additionally, purified proteins were analyzed by native polyacrylamide gel electrophoresis (PAGE) using stacking gel (3.75% of acrylamide) in 125 mM HEPES buffer pH 8.0, and resolving gel (9% of acrylamide) in 374 mM HEPES buffer at pH 6.5. The running buffer was prepared with HEPES 1% (m/v) and L-Histidine 1% (m/v), and the sample with the same stacking gel buffer supplemented with 20% glycerol (v/v) and 0.1 mg/mL methylene blue. Electrophoretic run were performed on a *Hoefer® SE600* series vertical slab gel electrophoresis unit (Hoefer, Inc., MA, USA) at 4 °C and 30 mA of constant current. The gel was stained with Coomassie blue and digitized for analysis.

HPLC purity analysis

The RP-HPLC was performed on a reverse phase column RP-C4 *UltraC4* (5 µm, 4.6x150 mm) (RESTEK, Bellefonte, PA, USA) at 37 ºC and 1 mL/min of flow in a HPLC *prominence UFLC Shimadzu* system (Shimadzu, Japan) consisted of a *CBM-20A* comunications modules, *DGU-20A5* degasser, LC-20AD liquid chromatography pump, SPD-20A UV/VIS detector, CTD-20A column oven and LC solutions program. The protein solution (20 µl, ~15 mg of protein) was injected into the column with a subsequent wash step using 5 mL of 0.1% trifluoroacetic acid (TFA) in water. The protein elution was then carried out with a linear gradient (30 min) from 0 to 100% acetonitrile in 0.1% TFA (Pazos *et al.* 2006). Absorbance at 225 nm (A_{225nm}) was used for monitoring the chromatography procedure.

Determination of the molecular physicochemical properties

Three physicochemical parameters were determined or estimated: molar extinction coefficient (ε_{280nm}), molecular weight (MW) and isoelectric point (pI).

Determination of the molar extinction coefficient and protein concentrations

The extinction coefficient was determined by plotting the absorbance at 280 nm (A_{280nm}) as a function of protein concentration (Valle *et al.* 2018). An *Ultrospec 4000* UV/Visible Spectrophotometer (*Pharmacia Biotech*, Suecia) was used to register the absorbance spectrum of each protein and the light scattering was corrected considering the absorbance at 350 nm (A_{350nm}). Protein concentration was determined by Lowry method (Lowry *et al.* 1951) using a standard bovine serum albumin solution (0.1-1 mg/mL (*Sigma*, Steinheim, Germany) and measuring the absorbance at 620 nm (A_{620nm}) in a *Multiskan EX* microplate reader (*Labsystems*, Finland).

Theoretical estimation of the molecular weight and isoelectric point

The theoretical MW and pI were estimated by ExPASy (*http://web.expasy.org/*) using the amino acid sequence of proteins. The experimental MW of pro-

teins was calculated from size-exclusion chromatography (SEC) on a *Superdex 75 10/300 GL increase* column (*GE Healthcare*, Chicago, IL, USA). The chromatography was performed isocratically at 0.8 mL/min on an *AKTA purifier* system (*GE Healthcare*, Chicago, IL, USA) using TBS buffer (10 mM Tris-HCl pH 7.4, 145 mM NaCl) and monitoring at A_{280nm}. Then, the MW of proteins was estimated from the calibration with protein gel filtration molecular weight markers.

Determination of the molecular weight by mass spectrometry

In addition, the proteins mass was assessed by MALDI-TOF mass spectrometry. The mass spectra were measured on an Autoflex Speed TOF/TOF (*Bruker Daltronics GmbH* Bremen, Germany) using nitrogen laser at 337 nm operated in linear positive mode with acceleration of 19 kV. Analysis were performed from 1 µL of purified protein mixed with 3 µL of a solution of α-Cyano-4-hydroxycinnamic acid (HCCA) prepared at 10 mg/ mL in TFA 0.1%/ acetonitrile 30%. The mixture was added directly onto MALDI target plate *MTP Ground Steel*. The equipment manipulation and result analysis were performed by the *Flex Control software v3.4*, and the theoretical masses were calculated using the Isotope *Pattern software v3.4* (Build 76, *Bruker Daltronics GmbH* Bremen, Germany).

Hemolytic activity assays

Hemolytic activity (HA) was performed as previously described (Valle *et al.* 2011). Briefly, turbidity of human red blood cells (HRBC) suspension was measured at 650 nm with a 96-well microplate reader *Multiskan EX* (*Labsystems*, Finlandia) upon addition of different amounts of protein. Protein were two-fold serially diluted in a flat-bottom 96-well microplate in a final volume of 100 µL of TBS and the assay started by adding the same volume of HRBC suspension, which concentration was adjusted to an apparent absorbance of 0.1 at 650 nm. The time course of hemolysis was followed for 15 min at room temperature and the hemolysis rate and percentage of hemolysis were determined using Eq.1 and Eq.2, respectivel

$$hemolysis\ rate\ (min^{-1}) = |slope\ curve| \quad (1)$$

$$hemolysis\ (\%) = \frac{(A_0 - A_{15min})}{(A_0 - A_{TX100})} \quad (2)$$

where $|slope\ curve|$ represents the absolute value of the linear slope from the time-dependent hemolysis curves, A_0 and A_{15min} represent the A_{650} nm at 0 and 15 min, respectively, and A_{TX100} the absorbance of the completely lysed HRBC by addition of 1 mM Triton X-100 (*Sigma-Aldrich*, St. Louis, MO, USA). In order to characterize the HA, the hemolysis rate and percentages of hemolysis were plotted as a function of protein concentrations and data adjusted to the sigmoidal Hill function to estimate the protein concentration necessary to achieve 50% of hemolysis rate (HR_{50}) and hemolytic activity (HC_{50}).

Modeling of the three-dimensional structures

Ten chimera 3D models were constructed by homology modeling using the MODELLER software v9.10 (Webb and Sali 2014) and the template structures of n◦1 and n◦2 StI NMR models (PDB 2KS4) (Castrillo *et al.* 2009) and StII X-ray crystallography structures (PDB 1GWY, chains A and B) (Mancheño *et al.* 2003). The statistical potential method, *Discrete Optimized Protein Energy* (DOPE), implemented in MODELLER, was used to assess the quality of structures modeled by homology. Aditionally, the stereochemical quality of protein structure models was analyzing using PROCHECK web server (*https://servicesn.mbi.ucla.edu/PROCHECK/*) (Laskowski *et al.* 1993). The exposure degree of residues was estimated with the WHAT IF server (*http://swift.cmbi.ru.nl/servers/html/index.html*). This algorithm calculates the average accessible surface area (ASA) as the accessible molecular surface of the amino acid X in the protein structural model relative to a Gly-X-Gly tri-peptide in vacuum.The visual analysis of protein structural models and the calculation of root-mean-square deviation (r.m.s.d.) of atomic positions were carried out using PyMol (*http://www.pymol.org*) and Chimera v1.10.1 (Pettersen *et al.* 2004) software. The geometrical characterization of protein-protein interfaces was performed with PDBePISA web server (*http://www.ebi.ac.uk/pdbe/pisa/*).

RESULTS

Expression and purification of sticholysins chimeric forms

The expression pET3a vectors of chimeric sticholysins were used to transform three *E. coli* strains: BL21(DE3), BL21(DE3)pLysS and BL21(DE3) pLysE, to select the best bacterial system. The chi-

meras were expressed by auto induction method (Studier 2005) in culture of 50 mL from five colonies of each three different strains. The results were examined by SDS-PAGE using standard molecular weights. The chimeric proteins were produced in the three *E. coli* strains with variable expression (Fig.2). It is possible to notice that stI_mid(stII) gene showed the highest expression levels with respect to total bacterial proteins in all the assessed strains (18-25%), whereas stII_Ct(stI) gene displayed the lowest expression (6-9% of total proteins) (Fig.2 and inset table).

After expression, bacterial cells were disrupted by sonication and the chimeric proteins were found after centrifugation mostly in the inclusion bodies fraction, as estimated from SDS-PAGE analysis (Fig.2B). Only 36-43% of the expressed proteins was soluble, similar to previous reports(Anderluh *et al.* 1996; de los Ríos *et al.* 2000; Wang *et al.* 2000; Jiang *et al.* 2002; Uechi *et al.* 2005; Pazos *et al.* 2006; Valle *et al.* 2016). Several colonies of the *E. coli* strains with the highest soluble expression levels were used for production at 600 mL, obtaining similar results than 50 mL scale according to SDS-PAGE analysis (Fig.2 and inset table). Chimeric sticholysins were purified as described (Pazos *et al.* 2006) by one-step cation-exchange chromatography on carboxymethyl-cellulose column and for all proteins a single symmetrical elution peak with hemolytic activity was obtained (Fig.3A). The highest protein yield values (109-278 mg of pure protein per liter of culture) were observed when the expression was performed in BL21(DE3)pLysS and BL21(DE3)pLysE *E. coli* strains (Fig.2 and inset table). These results indicate that the *E. coli* strains with additional T7-lac expression control by lysozyme are the most suitable bacterial systems for chimeric sticholysins production, similar to previously reported (Pazos *et al.* 2006; Valle *et al.* 2011; Hervis *et al.* 2014; Hervis *et al.* 2019). The homogeneity of protein samples was verified by SDS-PAGE (inset, Fig.3A) where the presence of a single band of ≈20 kDa was identified. The purity percentage was determined by RP-HPLC (Fig.3B) and all chimeric sticholysins were obtained with >98% purity by the one-step purification procedure routinely used for sticholysins and their Cys mutants (Pazos *et al.* 2006).

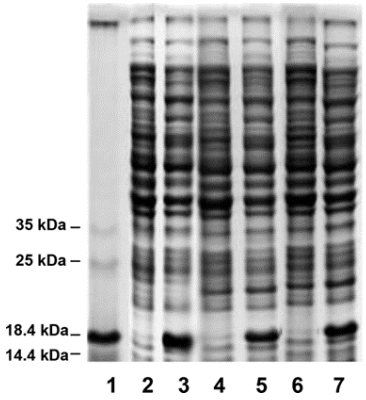

E. coli strain	chimeric sticholysin genes	Expression level (%)*	Solubility (%)**	Protein yield mg/L***
BL21(DE3)	*stI_Nt(stII)*	11.9 ± 2.0	39 ± 1.8	64
	stI_mid(stII)	24.5 ± 7.0	31.5 ± 0.7	93
	stII_Ct(stI)	7.8 ± 1.2	43 ± 1.4	35
BL21(DE3) pLysS	*stI_Nt(stII)*	14.2 ± 5.4	37 ± 1.4	109
	stI_mid(stII)	25.3 ± 1.5	42.3 ± 1.3	278
	stII_Ct(stI)	9.2 ± 2.5	38.5 ± 0.9	141
BL21(DE3) pLysE	*stI_Nt(stII)*	10.3 ± 0.6	37.5 ± 2.1	85
	stI_mid(stII)	18.0 ± 1.7	36.5 ± 0.7	165
	stII_Ct(stI)	6.3 ± 0.5	36.2 ± 0.3	121

Figure 2. Assessment of proteins expression and purification. Analysis by SDS-PAGE (12%) (Laemmli, 1970) of protein expression in *E. coli BL21 (DE3)pLysS* strain using the auto induction method (Studier, 2005). Lane 1: Pierce™ unstained protein molecular weight marker (Thermo Scientific, Waltham, MA, USA); lanes 2, 4, and 6: total proteins from non-induced cells transformed with the *pEt3a* expression vector of StI_Nt(StII), StI_mid(StII), and StII_Ct(StI), respectively. Lanes 3, 5, and 7: total proteins from induced cells transformed with the *pEt3a* expression vector of StI_Nt(StII), StI_mid(StII), and StII_Ct(StI), respectively. Inset table: Expression and purification parameters of chimeric proteins using three *E. coli* strains. *Percentage of chimeric sticholysins with respect to *E. coli* total protein. ** Percentage of soluble chimeric sticholysins with respect to the total chimeric protein produced. *** Purification yield of proteins expressed in mg of pure protein per liter of culture. Five colonies from each strain were used for genes expression studies.

Figura 2. *Evaluación de la expresión y purificación de las proteínas. Análisis por SDS-PAGE (12%) (Laemmli, 1970) de la expresión de las proteínas en la cepa E. coli BL21(DE3)pLysS mediante el método de autoinducción (Studier, 2005). Carril 1: marcador de peso molecular Pierce™ unstained protein molecular weight marker (Thermo Scientific, Waltham, MA, USA); carriles 2, 4 y 6: proteínas totales de las células no inducidas, transformadas con el vector de expresión pEt3a de StI_Nt(StII), StI_mid(StII) y StII_Ct(StI) respectivamente. Carriles 3, 5 y 7: proteínas totales de células inducidas transformadas con el vector de expresión pEt3a de StI_Nt(StII), StI_mid(StII) y StII_Ct(StI), respectivamente. Tabla insertada: parámetros de expresión y purificación de las proteínas quiméricas utilizando las tres cepas de E. coli. *Porcentaje de las sticholysinas quiméricas con respecto a las proteínas totales de E. coli. **Porcentaje de la sticholysina quimérica soluble con respecto a la proteína quimérica total producida. ***Rendimiento de purificación de las proteínas expresado en mg de proteína pura por litro de cultivo. Se utilizaron cinco colonias de cada cepa para los estudios de expresión de los genes.*

The electrophoretic protein motility influenced by the different isoelectric point of proteins was assessed by native electrophoresis PAGE (inset, Fig.3B). Chimeric sticholysins have the same amount of basic amino acids residues and only differ in their negatively charged residues composition. StI_Nt (StII) has the highest theoretical pI (9.3) (Table 1) and elution conductivity from cation-exchange chromatography of 14.8 ± 0.2 mS/cm.

The net charge of this chimeric protein is more positive than the rest and therefore migrates further towards the negative electrode (inset, Fig.3B). Contrarily, StI_mid(StII) has the lowest of theoretical pI (≈8.65) (Table 1) and elution conductivity from cation-exchange chromatography (9.5 ± 0.7 mS/cm). Therefore, StI_mid(StII) has less positive charges and less electrophoretic migration to the anode (inset, Fig.3B).

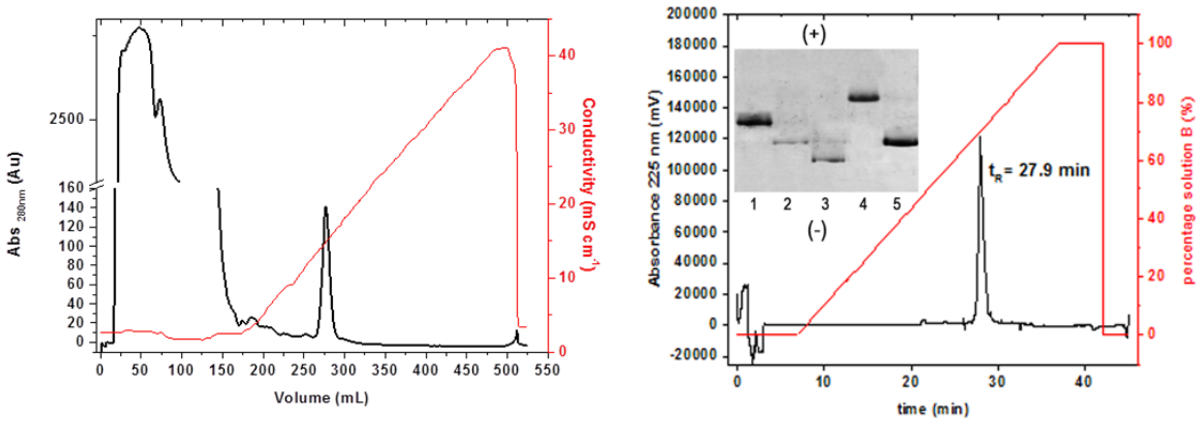

Figure 3. Purification of sticholysins chimeric forms. Typical cation-exchange chromatographic profile of chimeric StI_Nt(StII) sticholysin on a carboxymethyl cellulose (CM-52) column (1.6 x 20 cm) **(A)**. Purification was carried out from supernatant of lysed bacteria, as previously described (Pazos *et al.,* 2006), and monitored by the absorbance at 280 nm (Abs_{280nm}) (black line). The procedure was performed at 20.9 cm/h lineal flow and 6 mL fractions on *ÄKTAprimer plus* chromatography system (*General Electric*, Sweden) and proteins were eluted with a NaCl linear gradient which conductivity is represented (red line). **Inset (A):** Analysis of protein purification by SDS-PAGE (15%) (Laemmli, 1970). Lane 1: supernatant of lysed bacteria; lane 2: unbound protein fraction; lane 3: elution peak; and lane 4: Pierce™ unstained protein molecular weight marker (*Thermo Scientific*, Waltham, MA, USA). Typical RP-HPLC profile obtained from the CM-52 elution fraction on a Vydac reverse phase C4 column **(B)**, as previously described (Pazos *et al.,* 2006). The proteins homogeneity was determined from the peak integration. The RP-HPLC was performed with 0.1% trifluoroacetic acid (TFA) in water at 37 ºC and 1 mL/min flow in a prominence UFLC Shimadzu system (Shimadzu, Japan). The absorbance at 225 nm (black line) was used for monitored the chromatography. The proteins were centrifuged for 10 min at 10 000 xg, and ~15 µg of protein (in ≈20 mL) was injected into the column. The elution was carried out with a linear gradient of acetonitrile (red line) of 30 min using solution B consisting of 100% acetonitrile and 0.1% TFA. Similar results were obtained for the other chimeras. **Inset (B):** Analysis of purified proteins by native polyacrylamide gel electrophoresis PAGE (9%). Lane 1 and 2: StI and StII, molecular markets purified according Lanio *et al.,* (2001), respectively; lane 3: StI_Nt(StII); lane 4: StI_mid(StII); and lane 5: StII_Ct(StI).The polarity of the electrophoresis is positive (+) above and negative below (-).

Figura 3. *Purificación de las sticholysinas quiméricas. Perfil cromatográfico de intercambio catiónico típico de la sticholysina quimérica StI_Nt (StII) en una columna de carboximetilcelulosa (CM-52) (1,6 x 20 cm)* ***(A)****. La purificación se llevó a cabo a partir del sobrenadante de las bacterias lisadas, como se describió previamente (Pazos et al. 2006) y se monitoreó mediante la absorbancia a 280 nm (Abs_{280nm}) (línea negra). El procedimiento se realizó a un flujo lineal de 20,9 cm/h y fracciones de 6 mL en el sistema cromatográfico ÄKTAprimer plus (General Electric, Suecia) y las proteínas se eluyeron con un gradiente lineal de NaCl cuya conductividad se representa (línea roja).* ***Inserto (A)****: análisis de purificación de las proteínas por SDS-PAGE (15%) (Laemmli, 1970). Carril 1: sobrenadante de bacterias lisadas; carril 2: fracción de proteína no unida; carril 3: pico de elución; y carril 4: marcador de peso molecular de proteína Pierce™ unstained protein molecular weight marker (Thermo Scientific, Waltham, MA, USA). Perfil típico de RP-HPLC obtenido a partir de la fracción de elución de CM-52 en una columna C4 de fase inversa Vydac* ***(B)****, como se describió anteriormente (Pazos et al. 2006). La homogeneidad de las proteínas se determinó a partir de la integración del pico. La RP-HPLC se realizó con ácido trifluoroacético (TFA) al 0,1% en agua a 37ºC y flujo de 1 mL/min en un sistema UFLC Shimadzu (Shimadzu, Japón). Se usó la absorbancia a 225 nm (línea negra) para monitorear la cromatografía. Las proteínas se centrifugaron durante 10 min a 10000 x g y se inyectaron ~15 µg de proteína (en ~20 µL) en la columna. La elución se llevó a cabo con un gradiente lineal de acetonitrilo (línea roja), 30 min, utilizando la solución B compuesta de acetonitrilo al 100% y TFA al 0,1%. Se obtuvieron resultados similares para las otras quimeras.* ***Inserto (B)****: Análisis de las proteínas purificadas mediante electroforesis en gel de poliacrilamida nativa PAGE (9%). Carriles 1 y 2: StI y StII como marcadores moleculares purificados de acuerdo con Lanio et al., (2001), respectivamente; carril 3: StI_Nt(StII); carril 4: StI_mid(StII); y carril 5: StII_Ct(StI). La polaridad de la electroforesis es positiva (+) arriba y negativa debajo (-).*

Table 1. Molecular physicochemical properties of chimeric sticholysins.
Tabla 1. *Propiedades fisicoquímicas y moleculares de las sticholysinas quiméricas.*

	Parameters					
	$\varepsilon_{(mL\ mg^{-1}\ cm^{-1})}$		Theoretical**		SEC***	MS****
Proteins	ε_{280nm}	ε_{280nm}*	pI	MW (kDa)		MW (kDa)
St I	2.1 ± 0.1	1.92 ± 0.09	8.96	19.39	3.54	19. 39
St II	2.11 ± 0.04	1.99 ± 0.04	8.99	19.28	2.96	19.29
StI_Nt(StII)	2.16 ± 0.03	1.99 ± 0.03	9.30	19.27	2.50	19. 28
StI_mid(StII)	2.9 ± 0.1	2.26 ± 0.09	8.65	19.45	2.34	19. 46
StII_Ct(StI)	1.91 ± 0.03	1.84 ± 0.03	9.16	19.33	2.83	19. 34

* Extinction coefficient determined using the absorption value at 280 nm from the absorbance spectral (210-350 nm) corrected for scattering contributions. ** Theoretical parameters (isoelectric point and molecular weight) estimated by ExPASy server (*http://web.expasy.org/*). *** Experimental molecular weight estimated by size-exclusion chromatography (SEC***) and mass spectrometry (MS****).
Coeficiente de extinción determinado usando el valor de absorción a 280 nm a partir del espectro de absorbancia (210-350 nm) corregido con las contribuciones de dispersión. **Parámetros teóricos (punto isoeléctrico y peso molecular) estimados por el servidor ExPASy (http://web.expasy.org/). ***Peso molecular experimental estimado por cromatografía de exclusión molecular (SEC*) y espectrometría de masas (MS****).*

On the other hand, StI has a low theoretical pI (8.96) (Table 1), elution conductivity from cation-exchange chromatography (8.5 mS/cm) and lower electrophoretic migration than StII and StII_Ct(StI) but slightly higher comparing to StI_mid(StII) (inset, Fig.3B). The conductivity at which sticholysins and chimeras elute and the different electrophoretic migration could represent a simple procedure for the specific identification of these proteins.

Molecular physicochemical properties of chimeric sticholysins

The molar extinction coefficient at 280 nm of the sticholysins and its chimeric variants was determined in order to accurately calculate the protein concentration for functional comparison experiment. The values were slightly different when the light scattering contribution was considered (Table 1). The extinction coefficient was similar for all the proteins, since Trp residues that contribute to the absorption of the proteins at 280 nm were not modified. The MW of proteins was assessed by SEC (Table 1).

This chromatography could also detect the presence of putative sticholysins oligomers stabilized by electrostatic interactions, which are not stable during the SDS-PAGE and MALDI-TOF analysis. The Fig.4A shows the sticholysins SEC elution chromatograms obtained for proteins purified from cation-exchange carboxymethyl cellulose chromatography (Fig.3A). The elution volume for all proteins was similar (~17.4 ± 0.4 mL) (Fig.4A) corresponding to proteins of approximately 2.81 ± 0.42 kDa (Table 1) according to column calibration (Fig.4B). The presence of oligomers was dismissed, but the MW estimated by SEC is seven times lower than the ~20 kDa size theoretically calculated for these proteins (Table 1) and observed by SDS-PAGE (Fig. 2A and 3A, inset).

The underestimated MW could be related to protein interactions with the chromatographic resin, as has been previously reported when *Superdex* resins are used (Pentón *et al.* 2011; Laborde *et al.* 2017; Tanaka *et al.* 2017; Valle *et al*. 2018). The *Superdex 75 Increase* is a new generation of dextran- and agarose-based resins and a sugar binding site, which overlaps with the lipid binding site, was reported from the crystallographic structure of FraC-N-acetyl glucosamine complex (Tanaka *et al.* 2017). The actinoporin variants FraC W112R/W116F (Tanaka *et al.* 2017) and StI W111C (Valle *et al.* 2018), which amino acid subtitutions are located in the carbohydrate binding site,

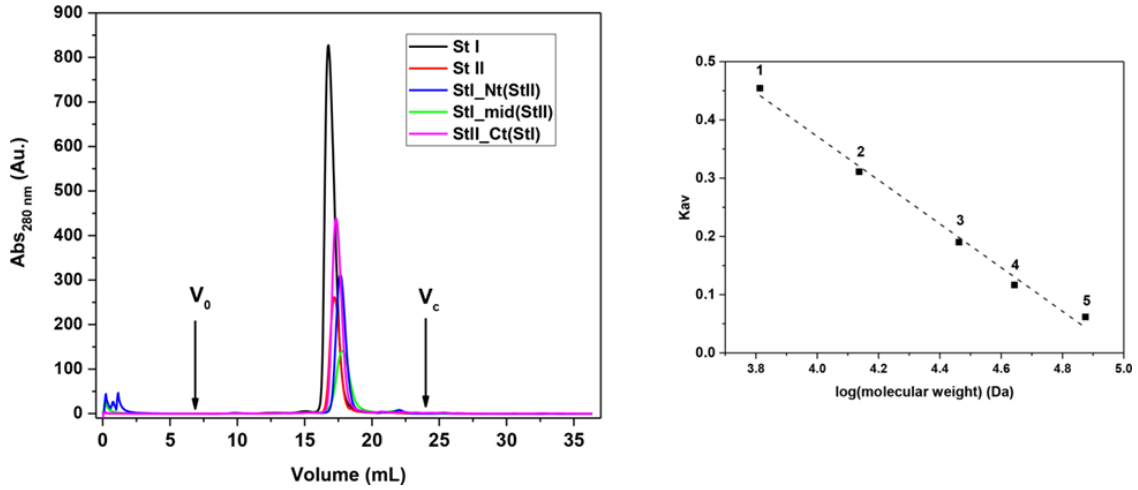

Figure 4. Molecular size-exclusion chromatography analysis. Size-exclusion chromatography (SEC) profiles of chimeric sticholysins on a *Superdex 75 Increase 10/300 GL* column (*GE Healthcare*, Chicago, IL, USA) at a flow rate of 0.8 mL/min **(A)**. Calibration curve of the SEC column plotted using the gel-phase distribution coefficient (Kav) versus logarithm of the molecular weight **(B)**. Kav = (V_e - V_0)/(V_c - V_0) where V_e = elution volume, V_0= void volume= 6.95 mL (based on blue dextran 2000 elution volume), V_c= bed volume= 24.04 mL. The V_0 and V_c are indicated with arrows. Marker proteins: 1, aprotinin (6.5 kDa); 2, ribonuclease A (13.7 kDa); 3, carbonic anhydrase (29 kDa); ovalbumin (44 kDa); 5, conalbumin (75 kDa). The equation of the linear fit (dashed line) was used to estimate the experimental molecular weights reported in Table 1.

Figura 4. *Análisis por cromatografía de exclusión molecular. Perfiles de la cromatografía de exclusión molecular (SEC) de las sticholysinas quiméricas en una columna Superdex 75 Increase 10/300 GL (GE Healthcare, Chicago, IL, EE. UU.) a un flujo de 0,8 mL/min* ***(A)****. Curva de calibración de la columna donde se grafica el coeficiente de partición (Kav) respecto al logaritmo del peso molecular* ***(B)****. Kav = (V_e - V_0)/(V_c - V_0) donde V_e=volumen de elución, V_0=volumen muerto=6,95 mL (basado en el volumen de elución del azul dextrano 2000), V_c=volumen de matriz=24,04 mL. V_0 y V_c se indican con flechas. Proteínas marcadoras de peso molecular: 1, aprotinina (6,5 kDa); 2, ribonucleasa A (13,7 kDa); 3, anhidrasa carbónica (29 kDa); ovoalbúmina (44 kDa); 5, conalbúmina (75 kDa). La ecuación del ajuste lineal (línea discontinua) se utilizó para estimar los pesos moleculares experimentales informados en la Tabla 1.*

displayed less interaction with SEC resins. In addition, the StIW111C dimerization by disulfide bridge also limited the access to the sugar (Valle *et al.* 2018). Therefore, the MW estimation by SEC chromatography is not reliable for the chimeric sticholysins. So, the MW of chimeric sticholysins was determined by MALDI-TOF and was similar to theoretically value (Table 1).

Hemolytic activity of sticholysins chimeric forms

The hemolytic activity (HA) of chimeric and wild-type sticholysins was evaluated by following the decay of turbidity of an HRBC suspension as a consequence of the cellular integrity loss upon protein addition. We estimated the maximum rate of hemolysis ($slope_{max}$), and the protein concentration necessary to achieve 50% of hemolysis rate (HR_{50}) (Fig.5A) and percentage of hemolysis (HC_{50}) (Fig.5B). As it is known, the activity of StII was higher and faster than the hemolysis elicited by StI (Lanio *et al.* 2001), as indicate the 33 and 8.5-fold lower values of HC_{50} and HR_{50}, respectively (Table 2, Fig.5).

In addition, the maximum hemolysis rate attained with StII is about two times higher than StI (Table 2, Fig.5A).

The hemolysis curves of the chimeric sticholysins occupated an intermediate position between those of StI and StII (Fig 5). In particular, the hemolytic activity of StI_Nt (StII) and StI_mid(StII) was 12-fold higher than StI and three-fold lower than StII (Table 2, Fig.5B). The maximum hemolysis rate was similar to StII for both chimeric proteins, but the HR_{50} parameter was two or three-fold higher, respectively (Table 2, Fig.5A). These results suggest that the exchange of the N-terminal and middle segments of StI by those of StII modifies the hemolytic activity of StI making it similar to the activity of StII. In the case of StII_Ct(StI), the $slope_{max}$ was identical to StII, with 1.7-fold higher HC_{50} value, and around 1.5-fold higher HR_{50} parameter. For this chimeric variant, the lytic activity is intermediate between StII and the rest of chimeric sticholysins, indicating that the exchange of the C-terminal segment of StII by the corresponding of StI maintains hemolysis rate, but it slightly reduces their pore-forming ability.

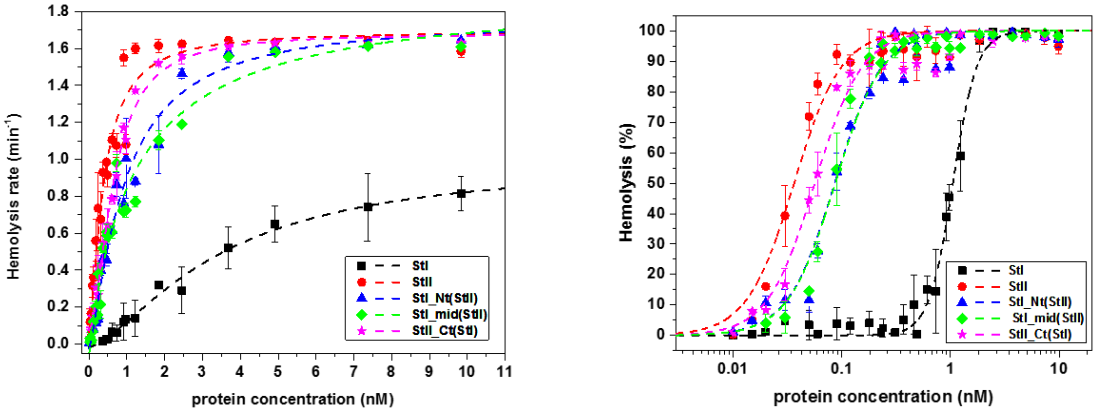

Figure 5: Hemolytic activity of chimeric sticholysins. Dose-dependence curves of the hemolytic rate **(A)** and the hemolysis percentage **(B)**. The time course of hemolysis was followed by the decrease in turbidity of an erythrocyte suspension adjusted to an initial apparent absorbance of 0.1 at 650 nm. Curves were fitted to a Hill function to calculate the parameters of the hemolytic activity shown in Table 2. Hemolysis rates were estimated from linear slopes of absorbance decrease and the HR_{50} (protein concentration needed to achieve 50% of maximum hemolysis rate) and showed in Table 2. HC_{50} (concentration of toxins where 50% of HRBC are lysed after 15 min) were calculated and showed in Table 2. Experiments were performed in triplicate and the mean values with the standard deviations are represented.

Figura 5: *Actividad hemolítica de las sticholysinas quiméricas. Curvas de la velocidad de hemólisis en dependencia de la dosis* ***(A)*** *y del porcentaje de hemólisis* ***(B)****. El proceso de hemólisis fue seguido por la disminución de la turbidez de una suspensión de eritrocitos ajustada a una absorbancia aparente inicial de 0,1 a 650 nm. Las curvas se ajustaron a una función de Hill para calcular los parámetros de la actividad hemolítica que se muestran en la Tabla 2. Las velocidades de hemólisis se estimaron a partir de pendientes lineales de disminución de la absorbancia y se calculó la HR_{50} (concentración de proteína necesaria para alcanzar el 50% de la velocidad máxima de hemólisis) Tabla 2. Se calculó el valor de HC_{50} (concentración de toxinas en la que se lisan 50% de HRBC después de 15 min) y se muestra en la Tabla 2. Los experimentos se realizaron por triplicado y se representan los valores medios con las desviaciones estándar.*

Table 2. Parameters of the hemolytic activity of chimeric sticholysins.

Tabla 2. *Parámetros de la actividad hemolítica de las sticholysinas quiméricas.*

Proteins	Parameters		
	HR_{50} (nM)	$slope_{max}$ (min^{-1})	HC_{50} (nM)
St I	3.4 ± 0.6	0.99 ± 0.13	1.07 ± 0.02
St II	0.40 ± 0.05	1.69 ± 0.07	0.032 ± 0.001
StI_Nt(StII)	0.9 ± 0.1	1.76 ± 0.09	0.090 ± 0.005
StI_mid(StII)	1.2 ± 0.3	1.91 ± 0.23	0.084 ± 0.002
StII_Ct(StI)	0.60 ± 0.03	1.68 ± 0.03	0.054 ± 0.003

HC_{50} and **HR_{50}**: protein concentration necessary to achieve 50% of hemolysis (Fig.5B) and hemolysis rate (Fig.5A), respectively. **$slope_{max}$**: maximum rate of hemolysis achieve in the assay.

HC_{50} *y* ***HR_{50}****: concentración de proteína necesaria para alcanzar el 50% de hemólisis (Fig.5B) y la velocidad de hemólisis (Fig.5A), respectivamente. pendiente$_{máx}$: velocidad máxima de hemólisis alcanzada en el ensayo.*

Structural model analysis

In order to explain the hemolytic activity results, ten models of the three chimeric sticholysins were constructed based on the determined structures for StI (Castrillo *et al.* 2009) and StII (Mancheño *et al.* 2003). The StII structure has the highest similarity between its chais A and B (PDB 1GWY) with r.m.s.d. of 0.09 Å, while the models n◦1 and n◦2 of StI NMR (PDB 2KS4) have r.m.s.d. of 0.6 Å. Also, the r.m.s.d. between StI and StII target structures used is 1.62 Å (Table 3). A representative 3D model for each chimera was selected based on the best quality criteria from the structural protein analysis.

Although the modeling by homology produces structures similar to the templates, the 3D models of chimeric sticholysins were more similar to StII (r.m.s.d. <0.33 Å) that to StI (r.m.s.d. <1.42 Å) (Fig.6) (Table 3), probably due to the high experimental precision of the crystallographic determination of StII structures.

Table 3. Structural comparison of models by r.m.s.d.
Tabla 3. *Comparación estructural de los modelos por r.m.s.d.*

r.m.s.d (Å)	target structures	
3D models	StI 2KS4 n◦1 and n◦2 models	StII 1GWY A and B chains
StI_Nt(StII)	1.42 ± 0.04	0.16 ± 0.01
StI_mid(StII)	0.93 ± 0.02	0.24 ± 0.01
StII_Ct(StI)	1.23 ± 0.07	0.33 ± 0.01
StI 2KS4 n◦1 and n◦2 models	0.626	1.62 ± 0.02
StII 1GWY A and B chains	1.62 ± 0.02	0.087

* r.m.s.d.: root-mean-square deviation of Cα atomic positions were calculated by PyMol software.
** r.m.s.d.: desviación cuadrática media de las posiciones atómicas Cα calculadas mediante el programa PyMol.*

The amino acid differences between StI and StII are represented in the N-terminal, middle and C-terminal segments of the chimeric models in Fig.6. The four amino acid differences (S1, E2A, D9A, E16Q, and G23E) between the N-terminal segments of StI and StII are showed in Fig.6A-C. The N-terminal segments folding in StI and StII 3D structures comprise the first 30 residues including the amphipathic helix-α1.

The structural modeling of this segment in all chimeras, including StI_mid(StII) (Fig.6B), which has residues of StI in this region (Fig.6A), showed greater structural similarity with StII (Fig.6C) than with StI (Table 3). The four amino acids that differ in the middle segments of StI and StII (V63F, S77D, S78T, and N95S) are showed in Fig.6D-F. The middle segments of sticholysins essentially participate in the β-sandwich folding and the membrane binding site. This segment in all chimeras, including StI_Nt(StII) (Fig.6E), which has residues of StI in this region, also showed greater structural similarity with StII (Fig.6F) than with StI (Fig.6D) (Table 3). The sticholysin C-terminal segment with the S121P, L134M, H147Y, and E148Q substitutions is involved in the β-sandwich folding and the membrane binding site, including the helix-α2 (Fig.6G-H). The accessible molecular surface of all substituted amino acids remained exposed or partially buried in each segment of the chimeric structures, according to ASA values higher than 20% (Table 4) (Gromiha *et al.* 1999). Only M134/135 from the C-terminal segment of StI_mid(StII) and StII_Ct(StI) (Fig.6G) are considered as buried (ASA <20%) (Table 4), since the helix-α2 conformational environments were modeled similarly to StII (Fig.6H). For the same reason, S76 and S77 from the middle segment of StI (Fig.6D) are considered as buried, but in the chimeric models (Fig.6E) these residues are exposed or partially buried.

Table 4. Degree of exposure of residues in structures and 3D models.
Tabla 4. *Grado de exposición de los residuos en estructuras y modelos 3D.*

	Accessible Surface Area (ASA)(%)						
	residues	**StI**	**StI_mid(StII)**	**residues**	**StI_Nt(StII)**	**StII**	**StII_Ct(StI)**
N terminal segment	**S 1**	60.0 ± 6.1	63.7 ± 5.7	**A 1**	54.0 ± 2.63	70.8 ± 0.7	63.5 ± 7.8
	E 2	51.7 ± 7.4	47.6 ± 7.5	**A 8**	41.5 ± 5.9	40.8 ± 1.7	44.0 ± 3.7
	D 9	46.1 ± 2.0	48.9 ± 1.8	**Q 15**	60.9 ± 7.0	64.1 ± 1.6	62.9 ± 4.0
	E 16	64.5 ± 4.5	63.7 ± 3.1	**E 22**	74.6 ± 10.6	72.1 ± 0.8	72.6 ± 6.8
	G 23	77.3 ± 3.5	73.8 ± 4.7				
	Accessible Surface Area (ASA)(%)						
	residues	**StI**	**StI_Nt(StII)**	**residues**	**StII**	**StI_mid(StII)**	**StII_Ct(StI)**
middle segment	**V 62/63**	50.3 ± 2.7	47.7 ± 5.1	**F 62/63**	56.3 ± 3.2	56.2 ± 5.8	56.6 ± 6.9
	S 76/77	13.3 ± 1.8	40.7 ± 5.7	**D 76/77**	39.4 ± 0.4	39.4 ± 5.3	36.5 ± 2.4
	S 77/78	55.8 ± 5.2	65.6 ± 7.6	**T 77/78**	72.4 ± 0.3	67.6 ± 2.3	72.3 ± 6.2
	N 94/95	58.5 ± 0.1	50.5 ± 4.0	**S 94/95**	65.8 ± 0.1	61.7 ± 5.3	64.4 ± 1.9
	Accessible Surface Area (ASA)(%)						
	residues	**StI**	**StI_Nt(StII)**	**StI_mid(StII)**	**StII_Ct(StI)**	**residues**	**StII**
C terminal segment	**P 121/122**	76.1 ± 6.4	55.0 ± 3.8	62.6 ± 3.4	63.6 ± 1.8	**S 121**	53.9 ± 0.3
	M 134/135	39.1 ± 3.2	17.9 ± 5.9	0.58 ± 0.5	1.1 ± 0.8	**L 134**	0.3 ± 0.4
	Y 147/148	41.8 ± 4.4	40.2 ± 1.2	41.0 ± 3.5	36.1 ± 2.2	**H 147**	25.4 ± 0.2
	Q 148/149	33.3 ± 6.0	48.2 ± 6.4	47.4 ± 6.6	45.3 ± 4.7	**E 148**	56.1 ± 5.2

The degree of exposure of residues in the 3D structures and models were calculated by Accessible Surface Area (ASA) as the accessible molecular surface of the amino acid (X) in the protein structural model relative to a Gly-X-Gly tri-peptide in vacuum. Five best models for each chimera were used to calculate the ASA average by WHAT IF server. StI (PDB 2KS4, M1 and M2) and StII (PDB 1GWY, chains A and B) structures were used. Amino acids with ASA values <20% are considered as buried; with 20%≤ ASA ≤50% as partially buried, and ASA >50% as exposed (Gromiha et al., 1999).
El grado de exposición de los residuos en las estructuras y modelos 3D se calculó mediante el área accesible a la superficie (ASA) definida como la superficie molecular accesible del aminoácido (X) en el modelo estructural de la proteína en relación con un tripéptido Gly-X-Gly en vacío. Se utilizaron los cinco mejores modelos para cada quimera en el cálculo del promedio de ASA con el servidor de internet WHAT IF. Se utilizaron las estructuras de StI (PDB 2KS4, M1 y M2) y StII (PDB 1GWY, cadenas A y B). Los aminoácidos con valores de ASA <20% se consideran ocultos; con 20%≤ ASA ≤50% como parcialmente ocultos y ASA >50% como expuesto (Gromiha et al. 1999)..

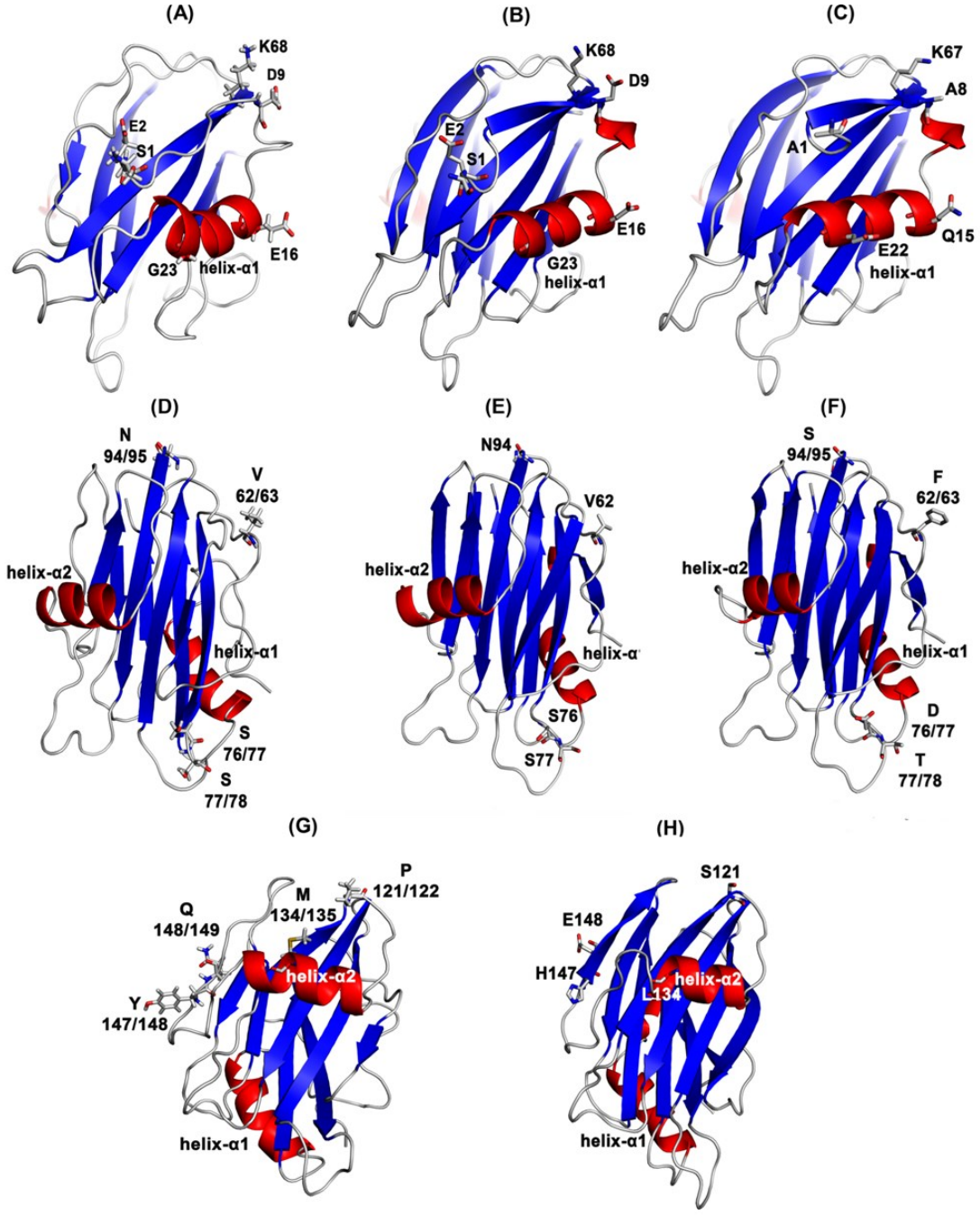

Figure 6. Structural models of chimeric sticholysins. The amino acids substitutions between the N-terminal segments of StI **(A),** StI_mid(StII) **(B)**, StII, StI_Nt(StII), and StII_Ct(StI) **(C)** chimeras are showed. The substtitions for the middle segments are represented for StI **(D)**, StI_Nt(StII) **(E)**, and for StII, StI_mid(StII), and StII_Ct(StI) **(F)** chimeras. The substitutions for C-terminal segments are represented for StI, StI_Nt(StII), StI_mid(StII) and StII_Ct(StI) **(G)**, and for StII **(H)**. The degree of exposure of residues in the 3D structures and models were calculate (Table 4). The Figure was generated using the MODELLER software v9.10.

Figura 6. *Modelos estructurales de las sticholysinas quiméricas. Se muestran las sustituciones de aminoácidos entre los segmentos N-terminales de StI* ***(A)****, StI_mid(StII)* ***(B)****, StII, StI_Nt(StII) y StII_Ct(StI)* ***(C)****. Para los segmentos intermedios, se representan StI* ***(D)****, StI_Nt(StII)* ***(E)****, StII, StI_mid(StII) y StII_Ct(StI)* ***(F)****. Las sustituciones en los segmentos C-terminales están representadas para StI, StI_Nt(StII), StI_mid(StII) y StII_Ct(StI)* ***(G)****, y para StII* ***(H)****. Se calculó el grado de exposición de los residuos en las estructuras y modelos 3D (Tabla 4). La figura se generó utilizando el programa MODELLER v9.10.*

DISCUSSION

Sea anemones produce actinoporin multigene families by several molecular mechanisms such as allelic polymorphism, alternative gene splicing, trans-splicing and gene duplication (Valle *et al.* 2015). The development of similar isotoxins with small functional differences might be an evolutionary strategy occurring in anemones to successfully explore the variety of preys encountered in the marine environment (Fatehi *et al.* 1994; Anderluh and Maček 2002). Actinoporins isoforms production has been confirmed in the most sea anemones species such as: *Actinia equina* (Macek and Lebez 1988; Anderluh *et al.* 1999), *Actinia tenebrosa (Galettis and Norton 1990; Norton et al. 1990)*, *Stichodactyla helianthus* (Lanio *et al.* 2001), *Heteractis crispa* (also called *Radianthus macrodactylus*) (Monastyrnaya *et al.* 2002; Klyshko *et al.* 2004), *Heteractis magnifica(Wang et al. 2000; Wang et al. 2008)*, *Oulactis orientalis* (Il'ina *et al.* 2005b; Il'ina *et al.* 2005a; Monastyrnaya *et al.* 2010), *Actinia fragacea* (Bellomio *et al.* 2009), *Actineria villosa,* and *Phyllodiscus semoni* (Uechi *et al.* 2010). The two isoforms of sticholysin reported exhibit 99% of similarity, 93% of identity (Huerta *et al.* 2001; Lanio *et al.* 2001) and consequently very similar 3D structures (Mancheño *et al.* 2003; Castrillo *et al.* 2009). Only 12 amino acid substitutions are responsible for the significant difference in terms of pore-forming activity (Martínez *et al.* 2001; Álvarez *et al.* 2009). In order to explain the lytic difference between StI and StII, we performed structure-function relationship studies. We designed and produced three chimeric sticholysin variants that exchange three segments: N-terminal, middle and C-terminal, with four amino acid substitutions each (Fig.1).

A structural model for each chimeric sticholysins was constructed by homology to complement the analysis of the experimental results and understand the functional implications of the amino acid differences between StI and StII. According to the calculed 3D models, most amino acid differences between StI and StII do not affect their solvent exposure, reflected by their accessible molecular surface area (Table 4). The predicted analysis suggested that none of the substitutions could be promoting conformational changes or interactions in the chimera 3D folding. Therefore, we will consider that the 3D structures of the chimeras are not different from those of StI and StII, although this question should be experimentally determined in immediate studies.

The mechanism for pore formation by actinoporins is not completely understood, but different regions of the protein plays important roles in the membranes interaction, oligomerization and final pore formation. According to the proposed pore formation mechanism for actinoporins, the N-terminal segment extends and inserts into the membrane forming the walls of the oligomeric pore (Tejuca *et al.* 1996; Hong *et al.* 2002; Malovrh *et al.* 2003; Gutierrez-Aguirre *et al.* 2004; Kristan *et al.* 2004; Alegre-Cebollada *et al.* 2007b; Tanaka *et al.* 2015; Valle *et al.* 2015). The greatest amino acid differences between StI and StII, and in general in the actinoporin family, are found in the N-terminal segment (Huerta *et al.* 2001; Lanio *et al.* 2001; Mancheño *et al.* 2003; Mechaly *et al.* 2011; Ros *et al.* 2015; Valle *et al.* 2015),(Mechaly *et al.* 2011; Ros *et al.* 2015; Valle *et al.* 2015). Particularly, several amino acid changes in the N-terminal segment and α-1 helix of actinoporins produced disturbance in the hydrophobicity profile that enhanced their hemolytic activity(Huerta *et al.* 2001; Ros *et al.* 2018). A single amino acid substitutions (E16Q and F15C) in StI wildtype produced protein variants conformationally similar to StI, but unexpectedly with greater hemolytic activity on HRBC and interaction with lipid monolayer than StI, respectively (Pazos *et al.* 2006; Valle *et al.* 2011). According to the structural assembly intermediate proposed to the 9-mer and 8-mer α-helical-bundle pores in FraC, these positions interact with the b-core region of another monomer during oligomerization (Mechaly *et al.* 2011; Tanaka *et al.* 2015; Valle *et al.* 2015). Also a single D9A and double E2A/D9A mutants of StI showed enhanced hemolytic activities (Rivera-de-Torre *et al.* 2017). The reverse mutation A8D in StII (equivalent D9A in StI) showed that this remplacement was enough to transform StII into a version with impaired pore-forming activity (Rivera-de -Torre *et al.* 2017).

The residue D9 of StI could be involved in a salt bridge with K68 (Fig.6A), equivalent to A8 and K67 positions in StII (Fig.6C) which are not able to electrostatically interact. The presence of this salt bridge that connects the N-terminal segment with the β-sandwich core, impaired the extension and detachment of this segment required for the formation of pores (Rivera-de-Torre *et al.* 2017), which leads to less lytic activity of StI. Our results are in agreement with this hypothesis since the chimeric proteins lacking this salt bridge, StI_Nt(StII) and StII_Ct(StI) (Fig.6C), displayed higher hemolytic activity than StI.

The hemolysis rate for these variants was similar to StII (Fig.5A and Table 2), whereas for StI_mid(StII) it was higher than the rest of the chimeric sticholysins, probably due to the presence of the salt bridge D9-K68 (Fig.6B). Considering the percentage of hemolysis, the activity of StI_mid(StII) and StI_Nt(StII) was the same (Fig.5B, Table 2). Therefore, the hypothesis of the salt bridge is not sufficient to explain the hemolytic activity differences between StI and StII. Other amino acid substitutions located in the middle segment (Fig.6D-F) could be determinant for the pore-forming activity.

The middle and C-terminal segments of sticholysins essentially participate in the β-sandwich folding, in the oligomerization and the membrane binding sites. Considering the high hemolytic activity of StI_mid(StII) in comparison to StI (Fig.5 and Table 2), the four substitutions between StI and StII (V63F, S77D, S78T and N95S) (Fig.6D-F) could be crucial to explain this functional difference. Since the participation of N95 of StI (Fig.7A) and S94 of StII (Fig.7C) residues have not been described in the membrane binding or oligomerization processes, we disregard their possible functional importance.

Residues V63 of StI (Fig.6D) and F62 of StII (Fig.6F), equivalents to R64 of FraC, are adjacent to E61/62, residues conserved in sticholysins and equivalent to H63 in FraC which has been proposed that participates in protein-protein interactions during oligomerization (Morante *et al.* 2015; Tanaka *et al.* 2015). Therefore, loss of positive charge and the hydrophobicity increase caused by the F63 substitution in StI_mid (StII), similar to F62 in StII (Fig.6F), could facilitate the oligomerization and lytic activity. The two residues S77/S78 in StI (Fig.6D) and D76/T77 in StII (Fig.6F) are located in a large loop. These residues are equivalent to N78/R79 of FraC which are positioned in the lipid binding site and also participate in protein-protein interactions into pore structure(Morante *et al.* 2015; Tanaka *et al.* 2015). In our opinion, the S77/78 substitution by T77/78 and in particulary, the non-conservative change S76/77 by D76/77, could be more important for defining the observed functional differences between StI, StII and StI_mid(StII). Thus, the enhanced StI_mid(StII) interaction with membrane and/or oligomerization could potentially increase its lytic activity to the same extent as StI_Nt (StII) (Fig.5), without eliminating the D9-K68 salt bridge (Fig.6B).

The four amino acids difference between StI and StII in the C-terminal segment (P122S, M135L, Y148H, and Q149E) (Fig.6G-H) are also responsible for the isoforms functional difference since the hemolytic activity of StII_Ct(StI) was slightly lower than StII (Fig.5). None of these residues have been proposed to participate in the pore formation mechanism. However, the two Y148/Q149 residues of StI (Fig.6G) and H147/E148 of StII (Fig.6H) are equivalent to H150/S151 of FraC, and contiguous to the conserved W146/147 residues in actinoporins, equivalent to W149 of FraC, which participates in the protein-protein interaction during the oligomerization process (Morante *et al.* 2015; Tanaka *et al.* 2015). Hence, the StII non-conservative changes H147/E148 by Y147/Q148 and the loss of charges could decrease the StII_Ct(StI) interaction with the membrane and/or the oligomerization and potentially reduce its lytic activity to an intermediate position between StII and StI_Nt (StII)/StI_mid(StII) (Fig.5).

We concluded that the three chimeric sticholysins displayed robust hemolytic activities but with intermediate values between StI and StII. Then, we speculate that several amino acid changes between the sticholysin isoforms are important for explaining their functional differences. In particular, the semi-conservative (V63 by F63 and S78 by T78) and non-conservative (S77 by D77) changes in StI could be partially responsible of the difference, for being involved in protein-membrane or protein-protein interactions during pore formation. Additionally, residues H147/E148 of StII are nearby to the protein-protein interface and could also explain the increased hemolytic activity of StII with respect to StI. So that, the salt bridge D9-K68 in StI is not sufficient to explain the functional differences between StI and StII isoforms.

Finally, the differences in aminoacidic composition that exist between the C-terminal segments are important for a preliminary explanation of the functional differences between these toxins. It appears that H147/E148 may be related to the high hemolytic activity of StII. However, much more efforts are needed to comparatively characterize the structure and membrane interaction ability of StI, StII and their chimeric variants. Increasing the available experimental data could shed light on the relationships between the structure and function of actinoporins.

Our rational protein design based in fragments has the advantage of being inexpensive since the number

of mutants is decreased to evaluate the single or co-operated contribution of the different amino acid substitutions between StI and StII. This approach can be accurate and reliably applied due to detailed and available knowledge of the structures and function of the sticholysins. From our results, specific mutants in the most important positions in determining the functional differences between StI and StII can be produced and characterized as a way of demonstrating our hypotheses. In particular, the semi-conservative (V63 by F62, S78 by T78, and Q149 by E148) and non-conservative (S77 by D77, and Y148 by H147) residues of StI by those of StII, respectively.

Acknowledgements

The purchase of synthetic genes was supported by the international project CAPES-MES N° 160/12 between Coordination for the Improvement of Higher Education Personnel (Coordenação de Aperfeiçoamento de Pessoal de Nível Superior, CAPES) and the Ministry of Higher Education of Cuba (Ministerio de Educación Superior, MES). We thank Dr. Prof. João Alexandre Ribeiro Gonçalves Barbosa and Dra. Prof. Sonia Maria de Freitas for the RP-HPLC and MALDI-TOF mass spectrometry analysis facilities in the Instituto de Ciencias Biológicas, Universidad de Brasília, DF -Brasília, Brasil. We are grateful to the graduate programs in Biochemistry and Molecular Biology at the University of Havana, Cuba.

CITED LITERATURE

Alegre-Cebollada, J., Onaderra, M., Gavilanes, J. G. and del Pozo, A. M. (2007a). Sea anemone actinoporins: the transition from a folded soluble state to a functionally active membrane-bound oligomeric pore. Curr Protein Pept Sci. 8(6): 558-72.

Alegre-Cebollada, J., Martinez del Pozo, A., Gavilanes, J. G. and Goormaghtigh, E. (2007b). Infrared spectroscopy study on the conformational changes leading to pore formation of the toxin sticholysin II. Biophys J. 93(9): 3191-201. https://doi.org/ 10.1529/biophysj.106.102566.

Álvarez, C., Mancheño, J. M., Martínez, D., Tejuca, M., *et al.* (2009). Sticholysins, two pore-forming toxins produced by the Caribbean Sea anemone Stichodactyla helianthus: their interaction with membranes. Toxicon. 54(8): 1135-47. https://doi.org/10.1016/j.toxicon.2009.02.022.

Anderluh, G., Krizaj, I., Strukelj, B., Gubensek, F., *et al*. (1999) Equinatoxins, pore-forming proteins from the sea anemone *Actinia equina*, belong to a multigene family. Toxicon. 37(10): 1391-401.

Anderluh, G. and Maček, P. (2002). Cytolytic peptide and protein toxins from sea anemones (Anthozoa: Actiniaria). Toxicon. 40(2): 111-24.

Anderluh, G., Pungercar, J., Strukelj, B., Macek, P., *et al.* (1996). Cloning, sequencing, and expression of equinatoxin II. Biochem Biophys Res Commun. 220(2): 437-42. https://doi.org/ 10.1006/bbrc.1996.0391.

Athanasiadis, A., Anderluh, G., Macek, P. and Turk, D. (2001). Crystal structure of the soluble form of equinatoxin II, a pore-forming toxin from the sea anemone Actinia equina. Structure. 9(4): 341-6. https://doi.org/ 10.1016/s0969-2126(01)00592-5.

Ávila, A. D., Calderon, C. F., Perez, R. M., Pons, C., *et al.* (2007). Construction of an immunotoxin by linking a monoclonal antibody against the human epidermal growth factor receptor and a hemolytic toxin. Biol Res. 40(2): 173-83.https://doi.org/S0716-97602007000200008.

Bakrač, B., Gutiérrez-Aguirre, I., Podlesek, Z., Sonnen, A. F.-P., *et al.* (2008). Molecular determinants of sphingomyelin specificity of a eukaryotic pore-forming toxin. Journal of Biological Chemistry. 283 (27): 18665-18677.

Bellomio, A., Morante, K., Barlic, A., Gutierrez-Aguirre, I., *et al.* (2009). Purification, cloning and characterization of fragaceatoxin C, a novel actinoporin from the sea anemone Actinia fragacea. Toxicon. 54(6): 869-80. https://doi.org/ 10.1016/j.toxicon.2009.06.022.

Belmonte, G., Menestrina, G., Pederzolli, C., Krizaj, I., *et al.* (1994). Primary and secondary structure of a pore-forming toxin from the sea anemone, Actinia equina L., and its association with lipid vesicles. Biochim Biophys Acta. 1192(2): 197-204.

Castrillo, I., Alegre-Cebollada, J., Martínez del Pozo, Á., Gavilanes, J. G., *et al.* (2009). 1H, 13C, and 15N NMR assignments of the actinoporin Sticholysin I. Biomolecular NMR Assignments. 3(1): 5. https://doi.org/ 10.1007/s12104-008-9127-3.

de los Ríos, V., Oñaderra, M., Martínez-Ruiz, A., Lacadena, J., *et al.* (2000). Overproduction in Escherichia coli and purification of the hemolytic protein sticholysin II from the sea anemone Stichodactyla helianthus. Protein Expr Purif. 18(1): 71-6. https://doi.org/ 10.1006/prep.1999.1174.

Fatehi, M., Rowan, E. G., Harvey, A. L. and Harris, J. B. (1994). The effects of five phospholipases A2 from the venom of king brown snake, Pseudechis australis, on nerve and muscle. Toxicon. 32 (12): 1559-72. https://doi.org/ 10.1016/0041-0101(94)90315-8.

Froger, A. and Hall, J. E. (2007). Transformation of plasmid DNA into E. coli using the heat shock method. Journal of visualized experiments: JoVE. 6).

Galettis, P. and Norton, R. S. (1990). Biochemical and pharmacological studies of the mechanism of action of tenebrosin-C, a cardiac stimulatory and haemolytic protein from the sea anemone, Actinia tenebrosa. Toxicon. 28(6): 695-706. https://doi.org/ 10.1016/0041-0101(90)90258-9.

García-Linares, S., Castrillo, I., Bruix, M., Menéndez, M., *et al.* (2013). Three-dimensional structure of the actinoporin sticholysin I. Influence of long-distance effects on protein function. Arch Biochem Biophys. 532(1): 39-45. https://doi.org/10.1016/j.abb.2013.01.005.

García-Linares, S., Rivera-de-Torre, E., Palacios-Ortega, J., Gavilanes, J. G., *et al.* (2017). The Metamorphic Transformation of a Water-Soluble Monomeric Protein Into an Oligomeric Transmembrane Pore. Chap. 2. In: Advances in Biomembranes and Lipid Self-Assembly. Elsevier Inc.

García, T., Martinez, D., Palmero, A., Soto, C., *et al.* (2009). Pharmacological effects of two cytolysins isolated from the sea anemone Stichodactyla helianthus. J Biosci. 34(6): 891-8. https://doi.org/ 10.1007/s12038-009-0103-6.

Gromiha, M. M., An, J., Kono, H., Oobatake, M., *et al.* (1999). ProTherm: Thermodynamic Database for Proteins and Mutants. Nucleic Acids Res. 27(1): 286-8. https://doi.org/10.1093/nar/27.1.286.

Gutierrez-Aguirre, I., Barlic, A., Podlesek, Z., Macek, P., *et al.* (2004). Membrane insertion of the N-terminal alpha-helix of equinatoxin II, a sea anemone cytolytic toxin. Biochem J. 384(Pt 2): 421-8. https://doi.org/ 10.1042/bj20040601.

Hervis, Y. P., Valle, A., Dunkel, S., Klare, J. P., *et al.* (2019). Architecture of the pore forming toxin sticholysin I in membranes. J Struct Biol.https://doi.org/ 10.1016/j.jsb.2019.07.008.

Hervis, Y. V., Valle, A., Canet, L., Álvarez, C., *et al.* (2014). Relevance of Pro80 for membrane interaction and pore formation by sticholysin I, a toxin from *Stichodactyla helianthus* (Anthozoa: Stichodactylidae). Rev. Cuba. Cienc. Biol. 3(2): 27-40.

Hinds, M. G., Zhang, W., Anderluh, G., Hansen, P. E., *et al.* (2002). Solution structure of the eukaryotic pore-forming cytolysin equinatoxin II: implications for pore formation. J Mol Biol. 315(5): 1219-29. https://doi.org/ 10.1006/jmbi.2001.5321.

Hong, Q., Gutierrez-Aguirre, I., Barlic, A., Malovrh, P., *et al.* (2002). Two-step membrane binding by Equinatoxin II, a pore-forming toxin from the sea anemone, involves an exposed aromatic cluster and a flexible helix. J Biol Chem. 277(44): 41916-24. https://doi.org/ 10.1074/jbc.M204625200.

Huerta, V., Morera, V., Guanche, Y., Chinea, G., *et al.* (2001). Primary structure of two cytolysin isoforms from *Stichodactyla helianthus* differing in their hemolytic activity. Toxicon. 39(8): 1253-6. https://doi.org/ 10.1016/s0041-0101(00)00247-6.

Il'ina, A. P., Monastyrsnaia, M. M., Sokotun, I. N., Egorov Ts, A., *et al.* (2005a). Actinoporins from the Sea of Japan anemone *Oulactis orientalis*: isolation and partial characterization. Bioorg Khim. 31 (1): 39-48.

Il'ina, A. P., Monastyrnaia, M. M., Isaeva, M. P., Guzev, K. V., *et al.* (2005b). Primary structures of actinoporins from sea anemone *Oulactis orientalis*.. Bioorg Khim. 31(4): 357-62.

Jiang, X. Y., Yang, W. L., Chen, H. P., Tu, H. B., *et al.* (2002). Cloning and characterization of an acidic cytolysin cDNA from sea anemone Sagartia rosea. Toxicon. 40(11): 1563-9. https://doi.org/ 10.1016/s0041-0101(02)00173-3.

Kem, W. R. (1988). Sea anemone toxins: structure and function. In: HESSINGER, D. A. and LENHOFF, H. M. (eds.) Biology of nematocysts. London: Academic Press.

Klyshko, E. V., Issaeva, M. P., Monastyrnaya, M. M., Il'yna, A. P., *et al.* (2004). Isolation, properties and partial amino acid sequence of a new actinoporin from the sea anemone *Radianthus macrodactylus*. Toxicon. 44(3): 315-24.

Kohno, Y., Satoh, H., Iguchi, A. and Nagai, H. (2009). Characterization of a new hemolytic protein toxin from the sea anemone *Anthopleura asiatica*. Fisheries Science. 75(4): 1049-1054.

Kristan, K., Podlesek, Z., Hojnik, V., Gutierrez-Aguirre, I., *et al.* (2004). Pore formation by equinatoxin, a eukaryotic pore-forming toxin, requires a flexible N-terminal region and a stable beta-sandwich. J Biol Chem. 279(45): 46509-17.

Laborde, R. J., Sanchez-Ferras, O., Luzardo, M. C., Cruz-Leal, Y., et al. (2017). Novel Adjuvant Based on the Pore-Forming Protein Sticholysin II Encapsulated into Liposomes Effectively Enhances the Antigen-Specific CTL-Mediated Immune Response. The Journal of Immunology. 198(7): 2772-2784.

Laemmli, U. K. (1970). Cleavage of structural proteins during the assembly of the head of bacteriophage T4. nature. 227(5259): 680-685.

Lanio, M. E., Morera, V., Álvarez, C., Tejuca, M., *et al.* (2001). Purification and characterization of two hemolysins from *Stichodactyla helianthus*. Toxicon. 39(2-3): 187-94.

Lanio, M. E. R., Molina, L. E. F., Quintana, R. J. L., Leal, Y. C., *et al.* (2014). Vaccine composition based on sticholysin encapsulated into liposomes. USA-patent US8697093B2(

Laskowski, R. A., MacArthur, M. W., Moss, D. S. and Thornton, J. M. (1993). PROCHECK: a program to check the stereochemical quality of protein structures. Journal of applied crystallography. 26 (2): 283-291.

Lowry, O. H., Rosebrough, N. J., Farr, A. L. and Randall, R. J. (1951). Protein measurement with the Folin phenol reagent. Journal of biological chemistry.

Macek, P. and Lebez, D. (1988). Isolation and characterization of three lethal and hemolytic toxins from the sea anemone Actinia equina L. Toxicon. 26(5): 441-51. https://doi.org/10.1016/0041-0101(88)90183-3.

Malovrh, P., Viero, G., Serra, M. D., Podlesek, Z., *et al.* (2003) .A novel mechanism of pore formation: membrane penetration by the N-terminal amphipathic region of equinatoxin. J Biol Chem. 278(25): 22678-85. https://doi.org/ 10.1074/jbc.M300622200.

Mancheño, J. M., Martin-Benito, J., Martínez-Ripoll, M., Gavilanes, J. G., et al. (2003). Crystal and electron microscopy structures of sticholysin II actinoporin reveal insights into the mechanism of membrane pore formation. Structure. 11(11): 1319-28.

Martinez, D., Otero, A., Alvarez, C., Pazos, F., *et al.* (2007). Effect of sphingomyelin and cholesterol on the interaction of St II with lipidic interfaces. Toxicon. 49(1): 68-81. https://doi.org/10.1016/j.toxicon.2006.09.019.

Martínez, D., Campos, A. M., Pazos, F., Álvarez, C., *et al.* (2001). Properties of St I and St II, two isotoxins isolated from *Stichodactyla helianthus*: a comparison. Toxicon. 39(10): 1547-60.

Mechaly, A. E., Bellomio, A., Gil-Carton, D., Morante, K., *et al.* (2011). Structural insights into the oligomerization and architecture of eukaryotic membrane pore-forming toxins. Structure. 19(2): 181-91. DOI: 10.1016/j.str.2010.11.013.

Monastyrnaya, M., Leychenko, E., Isaeva, M., Likhatskaya, G., *et al.* (2010). Actinoporins from the sea anemones, tropical *Radianthus macrodactylus* and northern *Oulactis orientalis*: Comparative analysis of structure-function relationships. Toxicon. 56(8): 1299-314. DOI: 10.1016/j.toxicon.2010.07.011.

Monastyrnaya, M. M., Zykova, T. A., Apalikova, O. V., Shwets, T. V., *et al.* (2002). Biologically active polypeptides from the tropical sea anemone *Radianthus macrodactylus*. Toxicon. 40(8): 1197-217. https://doi.org/ 10.1016/s0041-0101(02)00139-3.

Morante, K., Caaveiro, J. M., Viguera, A. R., Tsumoto, K., *et al.* (2015). Functional characterization of Val60, a key residue involved in the membrane-oligomerization of fragaceatoxin C, an actinoporin from *Actinia fragacea*. FEBS Lett. 589(15): 1840-6. https://doi.org/ 10.1016/j.febslet.2015.06.012.

Norton, R. S., Bobek, G., Ivanov, J. O., Thomson, M., *et al.* (1990) Purification and characterisation of proteins with cardiac stimulatory and haemolytic activity from the anemone *Actinia tenebrosa*. Toxicon. 28(1): 29-41.

Pardo-Cea, M. A., Castrillo, I., Alegre-Cebollada, J., Martínez-del-Pozo, Á., et al. (2011). Intrinsic local disorder and a network of charge-charge interactions are key to actinoporin membrane disruption and cytotoxicity. Febs j. 278(12): 2080-9. https://doi.org/ 10.1111/j.1742-4658.2011.08123.x.

Pazos, F., Valle, A., Martínez, D., Ramirez, A., *et al.* (2006). Structural and functional characterization of a recombinant sticholysin I (rSt I) from the sea anemone *Stichodactyla helianthus*. Toxicon. 48(8): 1083-94. https://doi.org/ 10.1016/j.toxicon.2006.09.004.

Pentón, D., Pérez-Barzaga, V., Díaz, I., Reytor, M. L., *et al.* (2011). Validation of a mutant of the pore-forming toxin sticholysin-I for the construction of proteinase-activated immunotoxins. Protein Engineering, Design & Selection. 24(6): 485-493.

Pettersen, E. F., Goddard, T. D., Huang, C. C., Couch, G. S., *et al.* (2004). UCSF Chimera–a visualization system for exploratory research and analysis. J Comput Chem. 25(13): 1605-12. https:// doi.org/ 10.1002/jcc.20084.

Ramírez-Carreto, S., Miranda-Zaragoza, B. and Rodríguez-Almazán, C. (2020). Actinoporins: From the Structure and Function to the Generation of Biotechnological and Therapeutic Tools. Biomolecules. 10(4). DOI: 10.3390/biom10040539.

Rivera-de-Torre, E., Palacios-Ortega, J., García-Linares, S., Gavilanes, J. G., *et al.* (2017). One single salt bridge explains the different cytolytic activities shown by actinoporins sticholysin I and II from the venom of *Stichodactyla helianthus*. Arch Biochem Biophys. 636(79-89. https://doi.org/ 10.1016/j.abb.2017.11.005.

Rojko, N., Kristan, K., Viero, G., Žerovnik, E., *et al.* (2013). Membrane damage by an α-helical pore-forming protein, Equinatoxin II, proceeds through a succession of ordered steps. J Biol Chem. 288 (33): 23704-15. https://doi.org/ 10.1074/jbc.M113.481572.

Ros, U., Rodríguez-Vera, W., Pedrera, L., Valiente, P. A., *et al.* (2015). Differences in activity of actinoporins are related with the hydrophobicity of their N-terminus. Biochimie. 116(70-8. https://doi.org/ 10.1016/j.biochi.2015.06.024.

Ros, U., Carretero, G. P. B., Paulino, J., Crusca, E., Jr., *et al.* (2018). Self-association and folding in membrane determine the mode of action of peptides from the lytic segment of sticholysins. Biochimie. 156(109-117. https://doi.org/ 10.1016/j.biochi.2018.10.005.

Studier, F. W. (2005). Protein production by auto-induction in high-density shaking cultures. Protein expression and purification. 41 (1): 207-234.

Tanaka, K., Caaveiro, J. M. M., Morante, K. and Tsumoto, K. (2017). Haemolytic actinoporins interact with carbohydrates using their lipid-binding module. Philos Trans R Soc Lond B Biol Sci. 372 (1726). https://doi.org/ 10.1098/rstb.2016.0216.

Tanaka, K., Caaveiro, J. M., Morante, K., González-Mañas, J. M., et al. (2015). Structural basis for self-assembly of a cytolytic pore lined by protein and lipid. Nature communications. 6(6337.

Tejuca, M., Serra, M. D., Ferreras, M., Lanio, M. E., *et al.* (1996). Mechanism of membrane permeabilization by sticholysin I, a cytolysin isolated from the venom of the sea anemone *Stichodactyla helianthus*. Biochemistry. 35(47): 14947-57. https://doi.org/ 10.1021/ bi960787z.

Tejuca, M., Anderluh, G. and Dalla Serra, M. (2009). Sea anemone cytolysins as toxic components of immunotoxins. Toxicon. 54(8): 1206-14. https://doi.org/ 10.1016/j.toxicon.2009.02.025.

Uechi, G., Toma, H., Arakawa, T. and Sato, Y. (2005). Molecular cloning and functional expression of hemolysin from the sea anemone Actineria villosa. Protein Expr Purif. 40(2): 379-84. https:// doi.org/ 10.1016/j.pep.2004.12.003.

Uechi, G., Toma, H., Arakawa, T. and Sato, Y. (2010). Molecular characterization on the genome structure of hemolysin toxin isoforms isolated from sea anemone *Actineria vil*losa and *Phyllodiscus semoni*. Toxicon. 56(8): 1470-6. https://doi.org/10.1016/ j.toxicon.2010.09.002.

Válcarcel, C. A., Dalla Serra, M., Potrich, C., Bernhart, I., *et al.* (2001). Effects of lipid composition on membrane permeabilization by sticholysin I and II, two cytolysins of the sea anemone *Stichodactyla helianthus*. Biophys J. 80(6): 2761-74. https://doi.org/ 10.1016/S0006-3495(01)76244-3.

Valle, A., Hervis, Y., Socas, L., Canet, L., *et al.* (2016) The multigene families of actinoporins (part II): Strategies for heterologous production in *Escherichia coli*. Toxicon. 118(64-81.

Valle, A., Pérez-Socas, L. B., Canet, L., Hervis, Y. P., *et al.* (2018). Self -homodimerization of an actinoporin by disulfide bridging reveals implications for their structure and pore formation. Sci Rep. 8(1): 6614. DOI: 10.1038/s41598-018-24688-2.

Valle, A., Alvarado-Mesén, J., Lanio, M., Álvarez, C., *et al.* (2015). The multigene families of actinoporins (part I): Isoforms and genetic structure. Toxicon. 103(176-187.

Valle, A., Lopez-Castilla, A., Pedrera, L., Martínez, D., *et al.* (2011). Cys mutants in functional regions of Sticholysin I clarify the participation of these residues in pore formation. Toxicon. 58(1): 8-17. https://doi.org/ 10.1016/j.toxicon.2011.04.005.

Wacklin, H. P., Bremec, B. B., Moulin, M., Rojko, N., *et al.* (2016). Neutron reflection study of the interaction of the eukaryotic pore-forming actinoporin equinatoxin II with lipid membranes reveals intermediate states in pore formation. Biochim Biophys Acta. 1858 (4): 640-52. https://doi.org/ 10.1016/j.bbamem.2015.12.019.

Wang, Y., Chua, K. L. and Khoo, H. E. (2000). A new cytolysin from the sea anemone, Heteractis magnifica: isolation, cDNA cloning and functional expression. Biochim Biophys Acta. 1478(1): 9-18. https://doi.org/ 10.1016/s0167-4838(99)00289-7.

Wang, Y., Yap, L. L., Chua, K. L. and Khoo, H. E. (2008). A multigene family of Heteractis magnificalysins (HMgs). Toxicon. 51(8): 1374-82. https://doi.org/ 10.1016/j.toxicon.2008.03.005.

Webb, B. and Sali, A. (2014). Comparative Protein Structure Modeling Using MODELLER. Current Protocols in Bioinformatics. John Wiley & Sons, Inc.

• • •